A Parameter Sweep Experiment on Topographic Effects on the Annular Variability

Seiya NISHIZAWA and Shigeo YODEN

Department of Geophysics, Kyoto University, Kyoto, Japan

(Manuscript received 29 January 2003, in final form 16 February 2004)

Abstract

Effects of surface topography on annular variability of the extratropical troposphere are examined by parameter sweep experiments with a simplified global circulation model. Amplitude of the sinusoidal surface topography h_m of zonal wavenumber m is swept as an experimental parameter in two series of experiments; a single zonal wavenumber, two ($m = 2$) or one ($m = 1$), is assumed in the series of WN2 or WN1, respectively. In additional series of WN2-1, the ratio of superposition of these two components is swept as an experimental parameter. In each run, long time integrations for 4300 days are done under a perpetual winter condition.

Characteristics of the leading mode of empirical orthogonal function (EOF) of the zonal-mean zonal wind, and the surface pressure (P_s), depend on the amplitude and zonal wavenumber of the surface topography. In the WN2 experiment, characteristics of EOF1 of zonal-mean zonal wind and P_s change dramatically around $h_2 = 450$ m, and the annular variability is divided into two types for large and small h_2. In the WN1 experiment, on the other hand, characteristics of the annular variability do not show such drastic changes as those in the WN2 experiment, and EOF1 of P_s shows annular pattern for all h_1 from 0 m to 1000 m.

Three typical cases are analyzed in detail; $h_2 = 0$ m (FLAT), $h_2 = 1000$ m (HWN2), and $h_1 = 1000$ m (HWN1). In the HWN2 experiment, the number of the storm tracks is two, and correlation map with the index that represents the oscillatory variability at that region shows a pattern localized in longitudes around the region with high teleconnectivity, even though EOF1 of P_s shows annular pattern.

On the other hand, the annular variability has a sound physical basis in the FLAT and HWN1 experiments. Importance of the number and spatial structure of storm tracks which exist at the exits of jet streams is also confirmed in the WN2-1 experiment.

1. Introduction

Thompson and Wallace (1998, 2000) and Thompson et al. (2000) pointed out that the leading mode of low-frequency variability of the extratropical circulation is characterized by "annular" structure in both of the Northern and Southern Hemispheres (hereafter NH and SH, respectively), so called "annular mode". The annular mode has almost zonally symmetric, and equivalent barotropic structure from the surface to the lower stratosphere. Yamazaki and Shinya (1999) showed that the annular mode is an internal mode of the atmosphere by a general circulation model (GCM) experiment with fixed external forcing parameters. The annular mode is associated with coupling between the zonal-mean zonal flow and eddies (Limpasuvan and Hartmann 2000; Hartmann et al. 2000; Kimoto et al. 2001). Baroclinic disturbances are most important in the SH, while planetary waves are also important in the NH.

The SH annular mode is basically the same phenomenon as the "zonal flow vacillation", which is caused by the interaction between the

Corresponding author: Seiya Nishizawa, Department of Geophysics, Kyoto University, Kyoto 606-8502, Japan.
E-mail: seiya@kugi.kyoto-u.ac.jp

zonal-mean zonal wind and baroclinic disturbances (e.g., Yoden et al. 1987; Hartmann 1995). In the NH, on the other hand, the temporal coherence between the Atlantic and Pacific mid-latitudes is weak, though the leading mode of empirical orthogonal function (EOF) of the sea-level pressure shows an annular pattern with the same sign in these regions (Deser 2000). In the EOF analysis, some uncorrelated variations may result in coherent structure in the leading mode (Ambaum et al. 2001; Itoh 2002). Ambaum et al. (2001) noted that the North Atlantic Oscillation (NAO), and the Pacific/North American (PNA) teleconnection patterns can be identified in a physically consistent way in the EOF analyses applied to various fields, but no such identification is found for the NH annular mode. The NH annular mode is not still understood physically, and relationship or independency between the NH and the SH annular modes is not clear.

Differences of the atmospheric low-frequency variability between the two hemispheres mainly result from the difference of the surface conditions, such as the topography and the land-sea thermal contrast. Taguchi and Yoden (2002) performed a parameter sweep experiment on the annular variability with an idealized global circulation model, in which only a sinusoidal surface topography of zonal wavenumber one was introduced, by changing its amplitude as an experimental parameter. They showed that the vertical linkage between the troposphere and the stratosphere in the annular variability depends on the amplitude of zonally asymmetric topography. However, they used only one horizontal pattern of the surface topography, though the real topography has not only zonal wavenumber one component, but also higher wavenumbers.

In this study, we further examine the effects of zonal asymmetry of the surface topography on the annular variability, by using a similar global circulation model with an idealized topography. First, two series of parameter sweep experiments are done with sinusoidal topography of zonal wavenumber two or one by changing its amplitude as the experimental parameter, in order to examine the dependence of annular variability on the amplitude of topography. Three typical cases of a flat surface, wavenumber one topography and wavenumber two are analyzed to examine difference in the annular variability from some viewpoints; subtropical westerly jet stream, storm track, teleconnectivity and so on. In addition, another series of parameter sweep experiment is done with superposed topography of zonal wavenumber one and two to clarify the relationship between the annular variability and storm track activity.

2. Model and experiment

The model used in this study is basically the same as the models used in Akahori and Yoden (1997) and Taguchi et al. (2001). The model is a simplified three-dimensional global primitive-equation model (Swamp Project 1998). A spectral-transform method is used for the horizontal advections, with a triangular truncation of the total wavenumber 42, and 30 σ-levels are adopted in the vertical discretization (Fig. 1a, right-hand side).

Some physical processes are simplified. Radiative processes are represented by a simple Newtonian heat/cooling scheme. The equilibrium temperature is assumed to be a winter condition in the NH, as shown in Fig. 1(a). The relaxation time-constant α is shown in Fig. 1(b); α^{-1} is 20 days in the troposphere except for the bottom two layers (5.5 and 12 days, respectively; Hoskins and Valdes 1990), while 4 days in the mesosphere. Rayleigh friction is used in the bottom boundary layer and the top sponge layer with the relaxation time-constant β shown in Fig. 1(b). All moist processes are removed for the model, and the dry convective adjustment scheme is retained. Internal horizontal dissipation in the ∇^4 form is applied to temperature, vorticity and divergence fields with a damping time of 6 hours for the maximum wavenumber, 42.

In the first two series of the experiments, sinusoidal surface topography is assumed only in the NH in the form of

$$h(\lambda,\phi) = \begin{cases} 4h_m \sin^2\phi(1-\sin^2\phi)\sin\left\{m\lambda - \frac{(2-m)\pi}{4}\right\} & \text{for } \phi \geq 0, \\ 0 & \text{for } \phi < 0, \end{cases} \quad (1)$$

where m is the zonal wavenumber, λ the longitude, and ϕ the latitude. The zonal wavenumber two or one is used in the WN2 or WN1

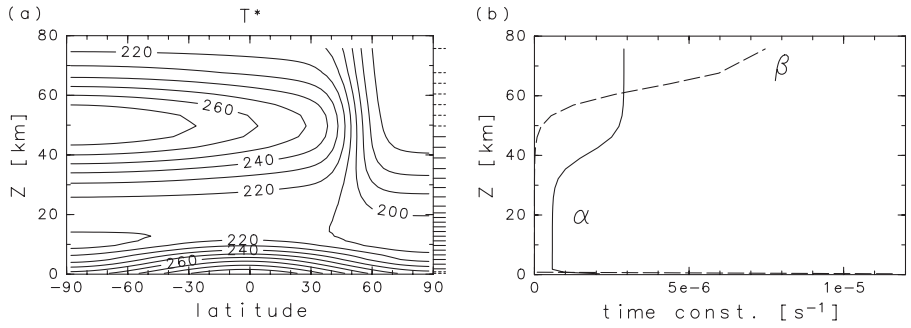

Fig. 1. (a) Radiative equilibrium temperature for Newtonian cool/heating and (b) relaxation time constant for Newtonian cool/heating α and that for Rayleigh friction β. Horizontal lines on the right-hand side of (a) denote the positions of vertical grids and dashed lines are those for bottom boundary layer and for top sponge layer.

experiment, respectively (Fig. 2). The amplitude of the topography h_m is swept as an experimental parameter from 0 to 1000 m (Table 1).

Another series of a parameter sweep experiment, WN2-1, is done to investigate the linkage between the WN2 and the WN1 experiments. The topography is given by

$$h(\lambda,\phi) = 4h_s \sin^2\phi(1-\sin^2\phi) \times \{(1-\mu)\sin(2\lambda) + \mu\sin(\lambda-\pi/4)\} \quad \text{for } \phi \geq 0, \tag{2}$$

where $h_s = 1000$ m. The parameter μ is changed from 0 to 1, as listed in Table 1.

Time integrations are done for 4300 days, from the initial state of an isothermal atmosphere (250 K) at rest, with small disturbances under the perpetual winter condition. Daily data of the last 4000 days are used in the present analysis after applying a low-pass filter of 30 days to remove high-frequency variations, such as baroclinic disturbances. We analyzed zonal wind, surface pressure P_s and geopotential height of 800 hPa or 1000 hPa. Because the results of geopotential heights are similar to those of P_s, we do not show the results of geopotential heights except for their time-mean.

3. Results

3.1 Parameter sweep in the WN2 and the WN1 experiments

An EOF analysis is done for the zonal-mean zonal wind field in the meridional cross section from 0° to 90°N, and from the surface to the

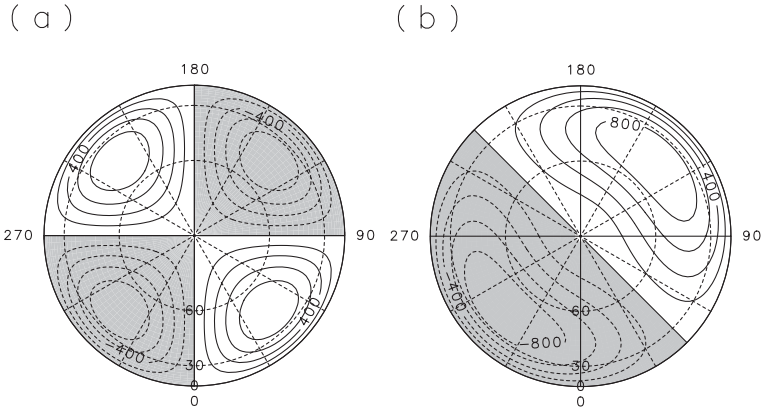

Fig. 2. Topography in (a) the WN2 experiment and (b) the WN1 experiment. Negative value is hatched. Number outside indicate longitude and number at longitude 0° indicate latitude.

Table 1. Experimental parameters h_m for the WN2 and the WN1 experiments and μ for the WN2-1 experiment.

	h_m
WN2	0, 200, 400, 450, 500, 550, 600, 800, 1000
WN1	0, 200, 400, 600, 800, 1000
	μ
WN2-1	0, 0.05, 0.1, 0.15, 0.2, 0.25, 0.3, 0.4, 0.6, 0.8, 1

50 hPa pressure level. For all the nine runs in the WN2 experiment, the leading mode (EOF1) has an equivalent barotropic structure with opposite sign between high- and mid-latitudes, as in the previous studies without topography (cf., Akahori and Yoden 1997). Latitudinal structure of the EOF1 pattern at 300 hPa is shown in Fig. 3 for nine h_2. The sign of EOF1 changes at about 60°N for $h_2 \leq 400$ m, while at about 50°N for $h_2 \geq 500$ m. There is a clear shift of the node between $h_2 = 400$ m and 500 m. Two other nodes in the subtropics also shift to lower latitudes at around $h_2 = 450$ m. These changes in the latitudinal structure of EOF1 are associated with the change in the latitudinal structure of the time- and zonal-mean zonal wind. It has a double jet structure with local maxima at about 55°N and 30°N for $h_2 \leq 400$ m, while a single jet structure at about 45°N for $h_2 \geq 450$ m. The most northern node of EOF1 is located at about 5° north of the jet, indicating the low-frequency fluctuation projected on EOF1, is associated with the latitudinal shift of the jet.

Contribution rate of the EOF1 mode for the zonal-mean zonal wind also shows large changes in the same parameter range of h_2 (Fig. 4). The rate is a little less than 60% for $h_2 = 0$ m, and decreases to about 30% for $h_2 = 400$ m. It becomes large for a small increment of h_2 around $h_2 = 450$ m, and is about 50% for $h_2 \geq 500$ m.

Spatial structure of EOF1 of the surface pressure P_s, has sensitive dependence on the topographic amplitude (Fig. 5), as well as on the latitudinal structure and the contribution rate of the EOF1 mode of the zonal-mean zonal wind. For $h_2 \leq 200$ m and $h_2 \geq 500$ m, the pattern is annular with opposite sign between the high- and mid-latitudes. On the other hand, it is not annular and wavenumber one component is dominant for $h_2 = 400$ m and 450 m. Similar pattern of zonal wavenumber one is found in EOF3 and EOF4 for $h_2 = 0$ m (the contribution rate is 9.8% and 8.9%, respectively) and EOF2 and EOF4 for $h_2 = 200$ m (the contribution rate is 13.9% and 9.6%, respectively), while EOF2s for $h_2 = 400$ m and 450 m are almost annular pattern, with zonal wavenumber two component (the contribution rate is 12.8% and 17.2%, respectively). Though the EOF1 pattern is annular both for small and large h_2, it has larger

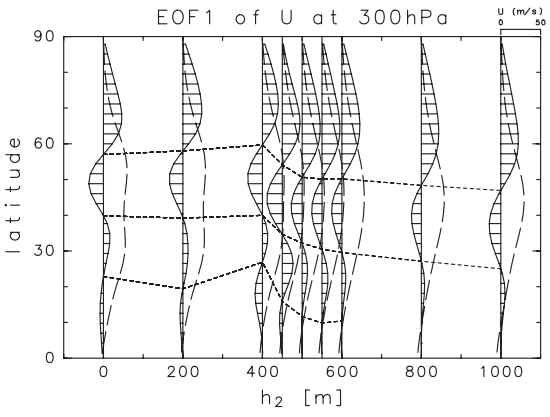

Fig. 3. Cross section of EOF1 of the zonal-mean zonal wind at 300 hPa (solid line) and the time- and zonal-mean zonal wind at the same level (broken line) depending on the amplitude of topography h_2.

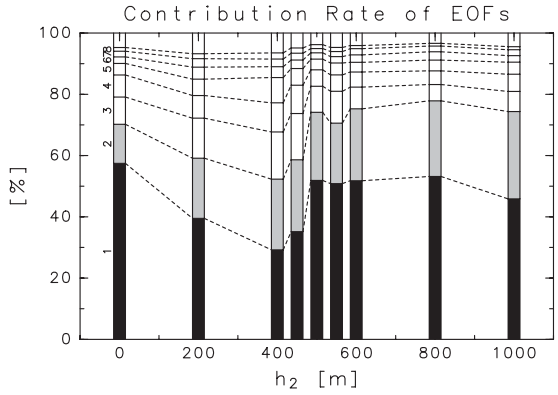

Fig. 4. Contribution rates of EOF1 of the zonal-mean zonal wind. The rate of the first mode, the second mode ..., up to the 8th mode are shown.

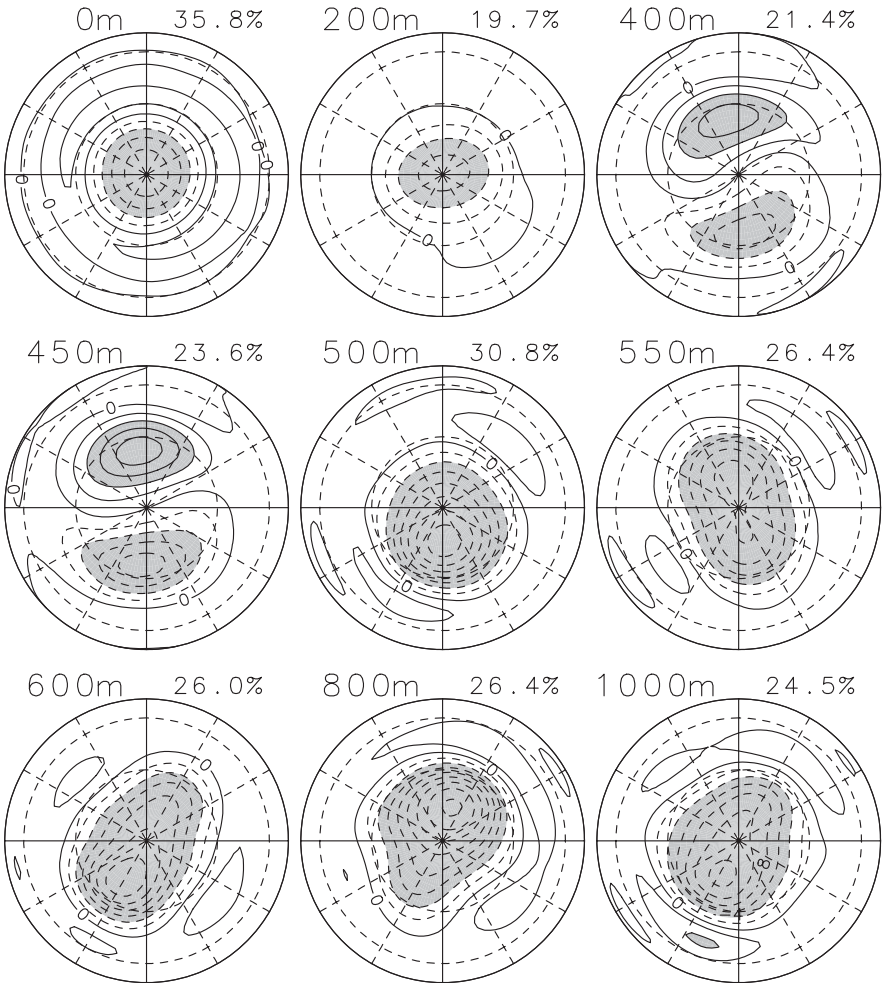

Fig. 5. The surface pressure P_s regressed on the standardized leading principal component in the WN2 experiment. Number on the top right in each panel represents the contribution rate. Contour interval is 2 hPa.

zonal asymmetry for large h_2; negative regions in the high-latitudes is elongated in the 150°–330° direction for $h_2 \geq 600$ m, while in the 30°–210° direction for $h_2 = 550$ m. Changes of the latitude of the most northern node and the contribution rate of the EOF1 mode of P_s, are similar to those of the EOF1 mode of the zonal-mean zonal wind, except for $h_2 = 400$ m and 450 m. Correlation between the leading principal components (PC1s) of the zonal-mean zonal wind and P_s is larger than 0.7, except for $h_2 = 400$ m and 450 m. Thus EOF1s of zonal-mean zonal wind and P_s, can derive a very similar component of the low-frequency variability of the extratropical troposphere, which is related with the latitudinal shift of the jet, in a wide parameter range of h_2, and the annular variability is strongly connected with the jet.

Annular variability in the WN1 experiment is also studied, with the same EOF analysis as described above. Latitudinal structure and contribution rate of EOF1 of the zonal-mean zonal wind, show similar characteristics to those of the WN2 experiment, but their dependency on the amplitude h_1 is weak. Figure 6 shows that EOF1 of P_s in the WN1 experiment is annular for all h_1, as in Taguchi and Yoden (2002). Zonal wavenumber one component, is also discernible in mid-latitudes for $h_1 \geq 400$ m. Note

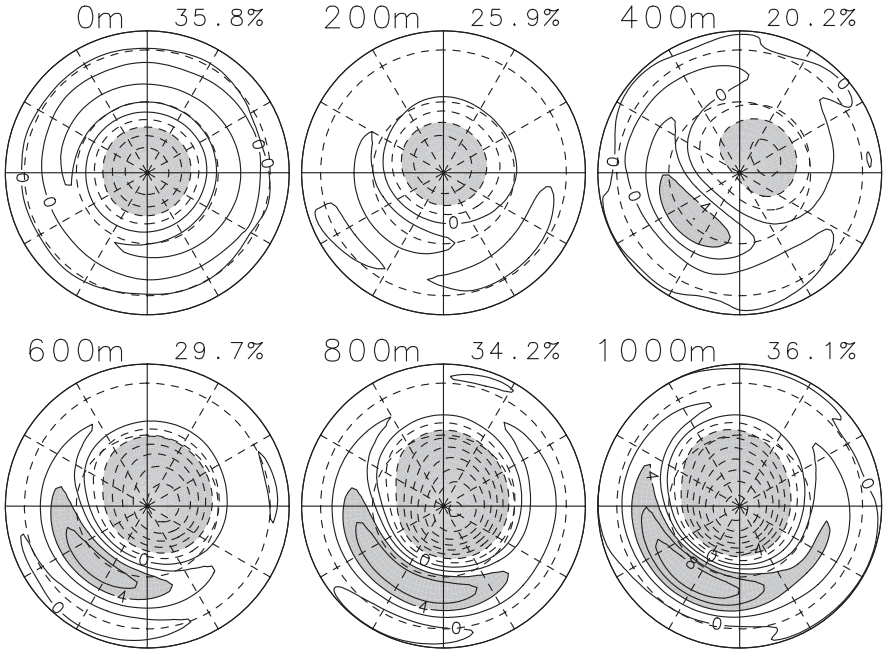

Fig. 6. Same as Fig. 5 but for the WN1 experiment.

that the drastic changes in the EOF1 pattern around 450 m in the WN2 experiment has no counter part in the WN1 experiment.

3.2 Three typical cases

Characteristics of the annular variability in the WN2 experiment is largely different between the runs for small h_2 and those for large h_2. It is also different between the large height runs in the WN2 experiment and those in the WN1 experiment. In this subsection, we focus on the following three cases; $h_2 = 0$ m, 1000 m of the WN2 and $h_1 = 1000$ m of the WN1 experiment (hereafter we denote FLAT, HWN2 and HWN1 experiments, respectively).

Figure 7 (top) shows the time-mean of the geopotential height of 800 hPa (Z800) and the variance of the surface pressure P_s. These patterns are zonally symmetric in the FLAT experiment. In the HWN2 and the HWN1 experiments, time-mean of P_s reflects the surface topography (not shown), and the climatological low of Z800 exists at the upstream and northern region of each topographical valley. The variance of P_s is large on the downstream region of the low, which is the pole side of each topographical valley; 150° and 330° in the HWN2 experiment, and 345° in the HWN1 experiment. The polar region is the saddle of the variance in the HWN2 experiment, while it is the region of large variance in the HWN1 experiment. The time-mean field of the zonal wind speed at 300 hPa (Fig. 7, bottom) shows locally intensified subtropical westerly jet streams in the HWN2 and HWN1 experiments. The number of the localized jet stream is identical to the zonal wavenumber of the topography. The exit of each jet stream is located near the bottom of the valley, and its longitudes coincide with those of the large variance of P_s, both for high- and low-frequency. These regions are the so called "storm tracks", and the number of storm tracks is also identical with the zonal wavenumber of the topography.

In order to extract teleconnection patterns (cf., Wallace and Gutzler 1981), one-point covariance analysis is done for the surface pressure field (Fig. 8, top). Pair of regions with large negative value of covariance, shows a zonally symmetric seesaw pattern between high- and mid-latitudes in the FLAT experiment. In the HWN2 experiment, two pairs of negatively large covariance are found, and they are located at storm tracks. The oscillatory

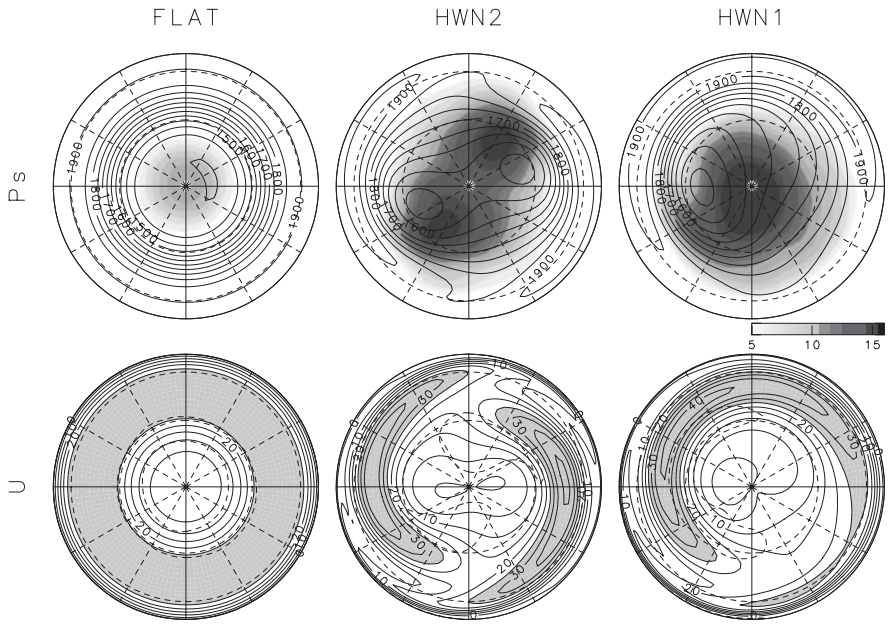

Fig. 7. Hemispheric patterns of [top] the time-mean of geopotential height of 800 hPa (contours) and the variance of the surface pressure (gray scale), and [bottom] the time-mean of the zonal wind speed at 300 hPa. The thick broken lines, which represent regions with large variance of high-frequency variability of P_s, are superimposed on bottom panels.

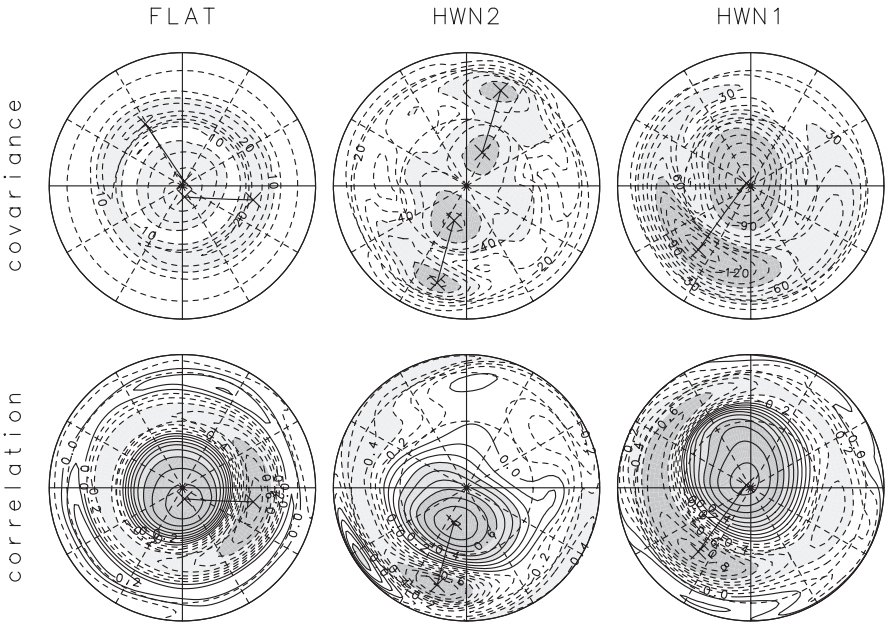

Fig. 8. Hemispheric patterns of [top] teleconnection map of the surface pressure derived by one-point covariance analysis and [bottom] correlation map for the index which is explained in the text. In the top panels, some pairs of points that have the largest negative covariance are shown by symbol $\times$ and connected by a thin line.

variabilities with large teleconnectivity are localized in longitudes. In the HWN1 experiment, on the other hand, only one pair is found, and its north-side region is in the polar region, and the opposite south-side region, centered at 320°, extends in longitudes widely.

After introducing an index which is the difference of normalized P_s with its standard deviation at the two points with the largest negative covariance, a correlation map of P_s with the index is made (Fig. 8 bottom). In the FLAT and the HWN1 experiments, the correlation pattern is annular and similar to the EOF1 pattern of P_s shown in Fig. 6. The region with high correlation is zonally elongated in mid-latitudes. Pattern correlations between the correlation pattern, and the EOF pattern in a sector ($\lambda_0 + 90° \leq \lambda \leq \lambda_0 + 270°$, $\phi \geq 30°$N; λ: longitude, λ_0: longitude of the southern point of the pair, ϕ: latitude), are -0.43 and -0.54 in the FLAT and the HWN1 experiments, respectively, and the correlation coefficient between PC1 of P_s and the index is -0.87 and -0.95, respectively.

In the HWN2 experiment, on the other hand, large value of the correlation is rather limited near the points to define the index. Correlation around 160° in mid-latitudes is near to 0, where EOF1 of P_s has a non-zero value with the same sign as that around 340° in mid-latitudes. The correlation pattern is zonally asymmetric, and not similar to the EOF1 pattern. Pattern correlation in the sector is -0.33, and correlation between the index1, that is calculated from the pair at about 340° and the PC1 of P_s is -0.77, while correlation between another index2, at about 160° and the PC1 is -0.57 (Table 2). These absolute values of the correlations are not so high as those in the FLAT or the WN1 experiment. Correlation coefficient between index1 and index2 is 0.07, and this value has no statistical significance. Thus variability at the two storm tracks is almost independent.

Table 2. Correlation between first three PCs and indices in the HWN2 experiment. Values are multiplied by 100.

	PC1	PC2	PC3
index1	−77	−11	51
index2	−57	35	−48
index1 + index2	−91	16	3
index1 − index2	−16	−33	73

3.3 *Parameter sweep in the WN2-1 experiment*

In order to examine the relationship between the annular variability and the storm track activity in more detail, another parameter sweep experiment WN2-1 is done, in which the ratio μ of the superposed topography of the zonal wavenumber one and two in Eq. (2) is swept from 0 to 1. Only the results for three cases of $\mu = 0.2, 0.4$ and 0.6 are shown here out of the eleven runs listed in Table 1. The topography is shown in the top of Fig. 9. As μ becomes large, the valley at 315° becomes wide while the other valley becomes shallow and then disappears. EOF1s of P_s (bottom of Fig. 9) have annular pattern for all μ, and wavenumber two component in mid-latitudes decreases, while wavenumber one component increases with μ. Contribution rate of the EOF1 mode becomes larger as μ increases.

Figure 10 shows the time-mean of Z800, the variance of P_s (top) and the time-mean field of the zonal wind speed at 300 hPa (bottom), similar to Fig. 7 for the FLAT, HWN2 and HWN1 experiments. For $\mu = 0.2$ and 0.4, there exist two jet streams and two storm tracks, and the variance around 180° becomes weak as μ becomes large. The number of jet streams, or storm tracks, changes to one for $\mu = 0.6$, and the storm track is wide in longitudes.

One-point covariance analysis is also done (Fig. 11, top). For $\mu = 0.2$ and 0.4, the pair with the largest negative covariance is located at almost the same longitude as the case of the HWN2 experiment. On the other hand, two points of the pair increase the distance over the pole for $\mu = 0.6$, and the region of large teleconnectivity in mid-latitudes is zonally elongated. In the same way as the previous subsection, index is calculated and correlation map of P_s, with the index is made (Fig. 11, bottom). For $\mu = 0.2$ and 0.4, large value of the correlation is limited near the points of the pair. Correlation around 180° in mid-latitudes is near to 0 where EOF1 of P_s has non-zero value with the same sign as that around 0°. For $\mu = 0.6$, the correlation map shows zonally

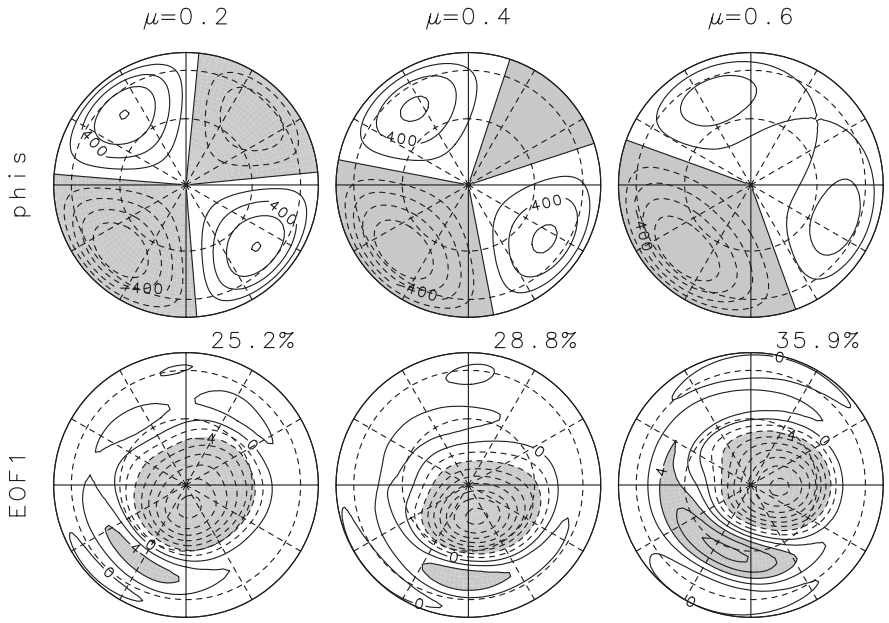

Fig. 9. Hemispheric patterns of [top] the topography and [bottom] the surface pressure regressed on the standardized leading PC. Left, center and right panel are the result in experiments for $\mu = 0.2, 0.4$ and 0.6, respectively. Number on the top right corner in each panel of bottom row represents the contribution rate.

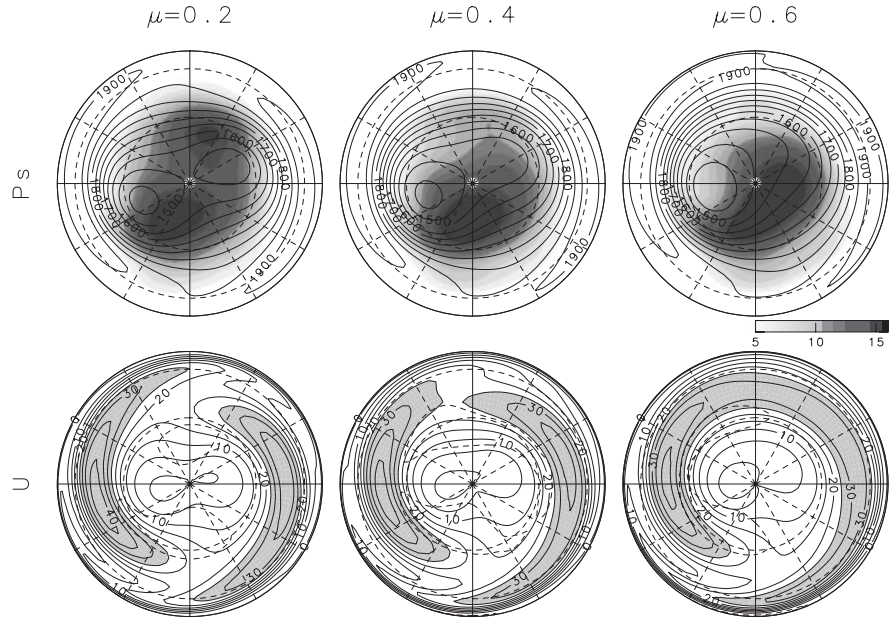

Fig. 10. Same as Fig. 7 but in the WN2-1 experiment.

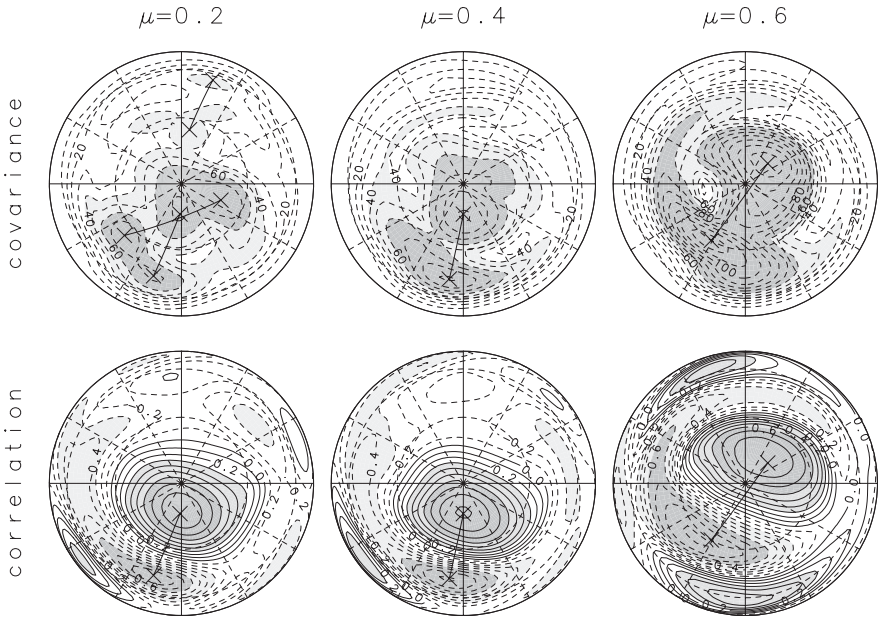

Fig. 11. Same as Fig. 8 but in the WN2-1 experiment.

elongated pattern in mid-latitudes, and it is similar to that of EOF1 of P_s, as the case of the HWN1 experiment.

In summary, some characteristics of the annular variability are different between $\mu = 0.4$ and 0.6, associated with the number and spatial structure of storm tracks.

4. Discussion

Figure 12 shows leading three EOFs of P_s in the FLAT experiment, the experiment for $h_2 = 450$ m, the HWN2 experiment and the HWN1 experiment. Some EOFs have an annular pattern, while some others have zonal wavenumber one pattern. In the FLAT experiment, there is a rotating zonal wavenumber one variability with a period of 40 days (EOF3 and EOF4, which is not shown). Zonal wavenumber one patterns of EOFs in the other experiments are related with the rotating zonal wavenumber one variability. In summary, low-frequency variabilities characterized in these EOFs in the series of the experiments are characterized mainly by the hemispheric annular pattern, the localized oscillatory pattern, or the zonal wavenumber one variability.

In order to explain the difference of EOF modes between the experiments, we use a simple five-component system which is similar to the three-component system introduced by Ambaum et al. (2001). This five-component system is basically the same as the three-component system, but is more similar to the variability in the present experiments. The five components shown in Fig. 13, right-bottom corner are considered; pole (P), two points in high-latitudes (AH, BH) and two points in mid-latitudes (AM, BM). Five time series a, b, c, d, and e, which are uncorrelated each other and have unit variance are introduced, and the five components are assumed as follows;

$$\begin{aligned}
P &= \alpha a + 0.5\gamma c + 0.5\delta d + \varepsilon e,\\
AH &= \alpha a + \beta b + \gamma c + \varepsilon e,\\
AM &= -\alpha a + \beta b - \gamma c - 0.5\varepsilon e,\\
BH &= \alpha a - \beta b + \delta d + \varepsilon e,\\
BM &= -\alpha a - \beta b - \delta d - \varepsilon e. \qquad (3)
\end{aligned}$$

The time series a represents purely annular variability; b represents zonal wavenumber one variability; c or d represents oscillatory variability between mid- and high-latitudes in localized longitudes around 135° or 315°, respectively, which affects the polar region weakly; and e represents oscillatory variability between

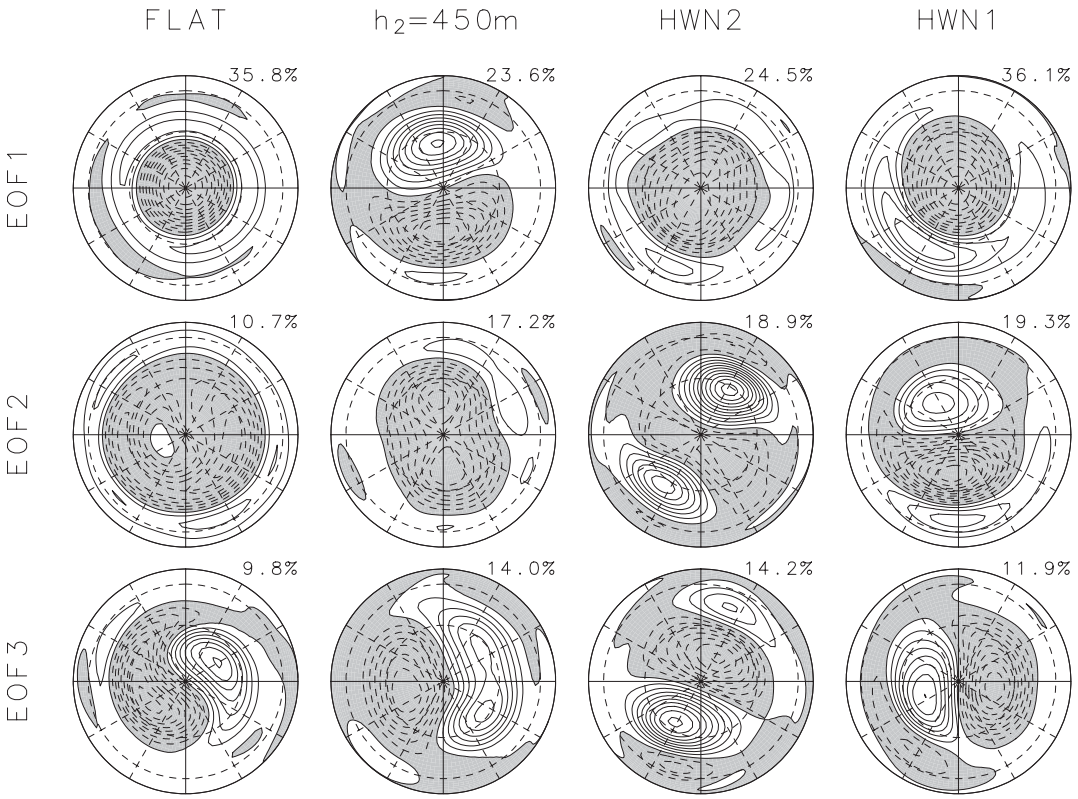

Fig. 12. First three EOFs of the surface pressure.

elongated longitudes centered 315° in mid-latitudes and the whole high-latitudes.

Now the following four cases are considered. In Case1, there are the annular and the zonal wavenumber one variabilities ($\alpha = 1$, $\beta = 0.5$ and the others are zero). In Case2, there are weak annular variability, the zonal wavenumber one variability and two localized oscillations ($\alpha = 0.5$, $\beta = 1$, $\gamma = 1$, $\delta = 1$ and $\varepsilon = 0$). In Case3, there are two localized oscillation ($\gamma = 1$, $\delta = 1$ and the others are zero). In Case4, there is one wide oscillation ($\varepsilon = 1$ and the others are zero).

Figure 13 shows the leading three EOF modes and their contribution rate in the four cases of the five-component system. In Case1, EOF1 shows the purely annular variability, and EOF2 shows the zonal wavenumber one mode. This is an ideal case of the FLAT experiment, in which EOF1 shows zonally symmetric pattern while EOF3 and EOF4 represents zonal wavenumber one pattern. Latitude of the minimum of EOF2 in the FLAT experiment is that of a node of the EOF1 pattern, and EOF2 has a role in the transition between positive PC1 phase and negative one; this result can be confirmed by the hodograph analysis in the PC1–PC2 phase space. In Case2, the first EOF shows the zonal wavenumber one mode, and EOF2 is an annular pattern. EOFs in Case2 have some similar properties to these for the WN2 experiment with $h_2 = 450$ m; EOF1 and EOF3 are zonal wavenumber one patterns, while EOF2 is an annular pattern with zonal wavenumber two component. EOF1 and EOF2 in Case3 is corresponding to EOF1 and EOF3 in the HWN2 experiment. Note that EOF1 in Case3 is obtained from two oscillations without purely annular variability ($\alpha = 0$). The hodograph analysis and the position of the node of the EOF1 show that EOF2 in the HWN2 experiment has a role in the transition between positive PC1 phase and negative one. Annular pattern with zonal wavenumber one component is naturally dominant in Case4, which corresponds to the HWN1 experiment. These results

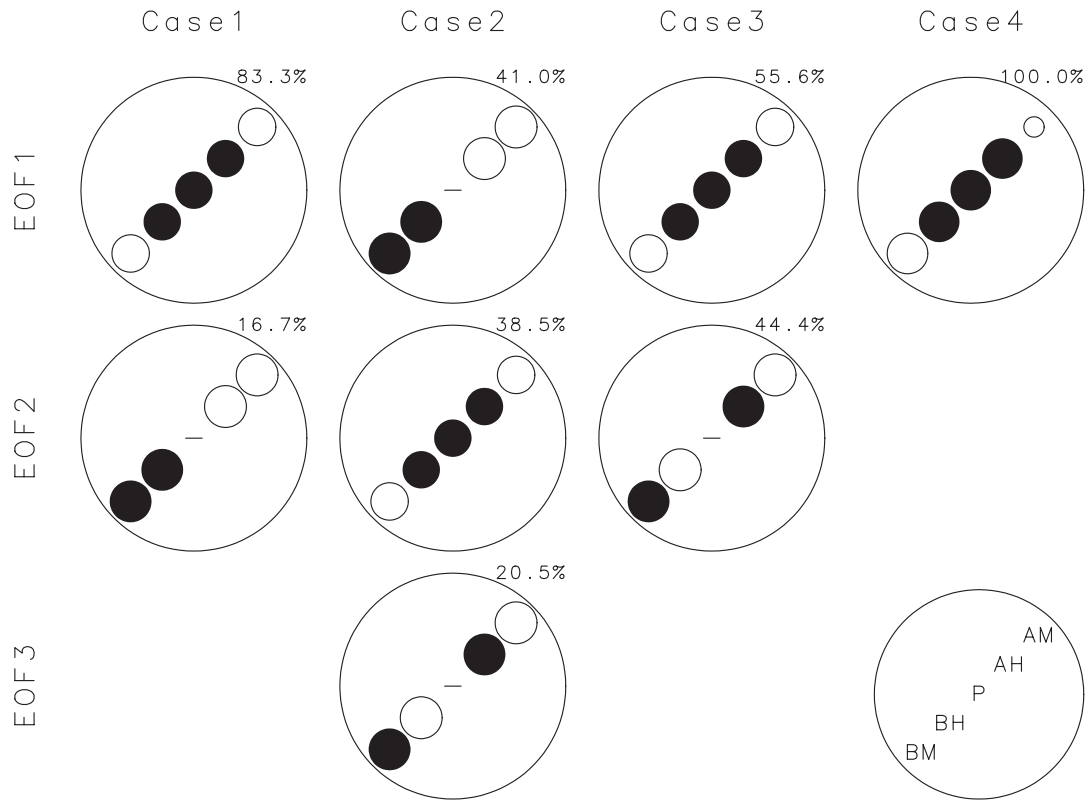

Fig. 13. First three EOFs in the five-component system. Size of circles relatively represent absolute value of EOF, and black and white ones denote negative and positive value, respectively. Horizontal lines represent zero.

show that this five-component system reproduces almost all dominant variabilities.

Now we consider the annular EOF1 in Case3, and in the HWN2 experiment. In Case3 of the five-component system, PC1 and PC2 is $-\sqrt{5}(c+d)/2$ and $-(c-d)$, respectively. Correlation between PC1 and $c+d$ is 1 and larger than correlation between PC1 and c, or that between PC1 and d. In the same way, correlation between PC2 and $c-d$ is 1 and larger than that between PC2 and c, or that between PC2 and d. As is shown in Table 2, for the HWN2 experiment, correlation of PC1 with index1 + index2 is larger than that with index1 or index2, and correlation of PC3 with index1 − index2 is larger than that with index1 or index2. Correlation maps of P_s for the index1 + index2 and index1 − index2 (Fig. 14) are very similar to EOF1 and EOF3, respectively (third column of Fig. 12). These results show the existence of a spurious annular mode due to the EOF analysis, for the case with two localized oscillations.

Additional EOF analysis in a quarter sphere is done to see the spurious character in the HWN2 experiment from a different view point. A quarter spheric data P_s^*, for an equivalent

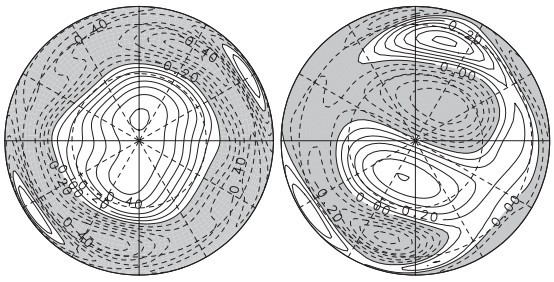

Fig. 14. Correlation map of P_s with index 1 + index2 (left) and with index1 − index2 (right) in the HWN2 experiment.

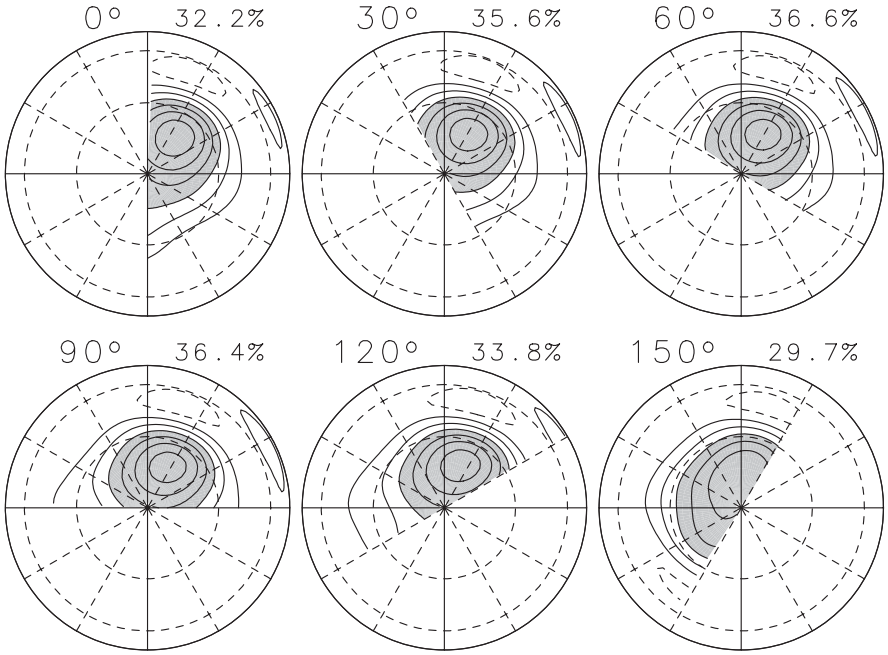

Fig. 15. EOF1 of P_s^* for $\lambda_0 = 0^\circ$ to 150° in the HWN2 experiment.

8000 days, is made from P_s for 4000 days as follows;

$$P^*_{sn^*}(\lambda,\phi) = \begin{cases} P_{sn^*}(\lambda,\phi), & 1 \le n^* \le n_{max} \\ P_{sn^*-n_{max}}(\lambda+180^\circ,\phi), & n_{max}+1 \le n^* \le 2n_{max} \end{cases}$$
$$\phi \ge 0, \quad \lambda_0 \le \lambda < \lambda_0 + 180^\circ, \quad n_{max} = 4000 \text{ days}. \tag{4}$$

The quarter spheric EOF analysis is done for six values of λ_0 from 0° to 150° with an increment of 30° (Fig. 15). For $\lambda_0 \le 120^\circ$, the large value region (with shade) is localized in longitudes at 150°, and the value at the pole is about half of the maximum. This pattern differs from the EOF1 pattern in the HWN2 experiment. Only for $\lambda_0 = 150^\circ$, EOF1 pattern is very similar to the hemispheric EOF1 of P_s (Fig. 5). Only when two storm tracks are contained in the region for EOF analysis, the obtained EOF1 shows annular pattern. This result gives another evidence that the annular EOF1 in the HWN2 experiment, is obtained from two storm tracks the same as in Case3 of the five-component system.

Generally EOF analysis tends to show too broad patterns, and its spatial orthogonality is sometimes a strong undesirable constraint (Cheng and Dunkerton 1995). As a result, EOFs are subject to inaccurate representation of the real physical relationship in the input data. Rotation of a subset of leading EOFs, known as rotated EOF, is often used to obtain spatial patterns that are more physically meaningful and statistically robust. Varimax rotation has been popular to obtain more localized patterns of variability. Varimax rotation was applied to the first eight EOFs for $h_2 = 1000$ m, and Fig. 16 shows the first two rotated EOFs (REOFs). The two patterns are almost point-symmetric. The REOF2 pattern and point-symmetry of the REOF1 pattern are similar as the correlation pattern (Fig. 8 bottom center), and the REOF1 pattern and point-symmetry of the REOF2 pattern are similar as the quarter spheric EOF patterns for $\lambda \le 120^\circ$ (Fig. 15). Unrotated EOF cannot show these patterns, because these are not spatially orthogonal to each other. When these patterns are on the physically meaningful bases, the constraint forces, unrotated EOF, to show spurious patterns; in this case it is an annular pattern.

Although the variability in this model is not identical to that in the real atmosphere, the

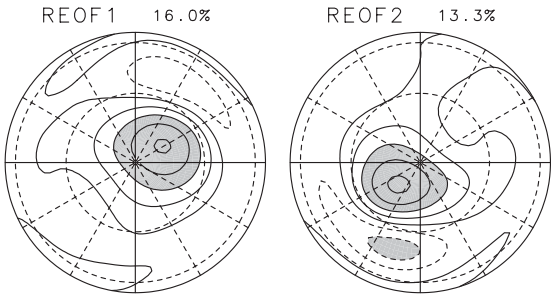

Fig. 16. Rotated EOF of P_s for $h_2 =$ 1000 m.

present result helps to think about the real atmosphere. In the real atmosphere, there are two storm tracks at the Pacific and the Atlantic regions in the NH due to large zonal asymmetry of topography, while less localized storm tracks in the SH due to small zonal asymmetry of topography. Thus the annular variability in the HWN2 experiment has similar characteristics to that in the NH, while that in the FLAT experiment is similar to that in the SH. There are also differences between the variability in the NH and in the HWN2: In the real atmosphere, latitudes of the two storm tracks are different. This difference may be important for the annular mode in the NH. On the other hand, in the HWN2 experiment, the latitudes are quite the same statistically.

5. Conclusions

The effects of topography on annular variability were studied by parameter sweep experiments with a simple global circulation model. EOF analyses of the zonal-mean zonal wind, and the surface pressure (P_s) fields, show that characteristics of the annular variability are sensitive to the amplitude and the zonal wavenumber of sinusoidal surface topography. In the WN2 experiment, EOF1 of P_s is not annular at $h_2 = 400$ and 450 m, while it is annular for other h_2. EOF1 of the zonal-mean zonal wind also shows large changes at the same parameter range of h_2. The annular variability in the WN2 experiment is divided into two types based on these characteristics for small and large h_2. In the WN1 experiment, on the other hand, EOF1 of P_s shows annular pattern for all h_1 and the dependence of annular variability on h_1 is small.

Three typical cases, FLAT ($h_2 = 0$ m), HWN2 ($h_2 = 1000$ m) and HWN1 ($h_1 = 1000$ m), are analyzed in detail. In the FLAT experiment, the variability of P_s is almost zonally symmetric. In the HWN2 experiment, two storm tracks are located at the exits of two subtropical westerly jet streams around two valleys. In the WN1 experiment, there is only one jet stream and storm track, and the variance of P_s is large over the polar region. The teleconnection pattern obtained by one-point covariance analysis is zonally symmetric in the FLAT experiment. There are two pairs of strong teleconnectivity localized around two storm tracks in the HWN2 experiment. In the HWN1 experiment, the number of the pair is one, and the north-side region of the pair is located in the polar region and the south-side region extends widely in longitudes. Correlation map with the index that shows oscillatory variability of the pair is annular and similar to the EOF1 pattern of P_s in the FLAT and the HWN1 experiments. On the other hand, in the HWN2 experiment, the correlation pattern is localized in longitudes around the pair and not similar to the EOF1 pattern. This means that the annular EOF1 is spurious.

In the WN2-1 parameter sweep experiment, the ratio of the superposed topography of the HWN2 and the HWN1 experiments is changed. When the number of jet streams and storm tracks is two, the spatial structure of the variability is similar to the case of the HWN2 experiment, i.e., spurious annular variability. On the other hand, when the number is one, the annular variability has a sound physical basis. Thus the structure of storm tracks are important factors to determine the annular variability.

Acknowledgments

The present graphic tools were based on the codes in the GFD-DENNOU library (SGKS Group 1999). Computations were performed on the VPP800 system of the Academic Center for Computing and Media Studies, Kyoto University. We are grateful for the comments from the three reviewers.

References

Akahori, K. and S. Yoden, 1997: Zonal flow vacillation and bimodality of baroclinic eddy life

cycles in a simple global circulation model. *J. Atmos. Sci.*, **54**, 2349–2361.

Ambaum, A.H.P., B.J. Hoskins and D.B. Stephenson, 2001: Arctic oscillation or North Atlantic oscillation? *J. Climate*, **14**, 3495–3507.

Cheng, X. and T.J. Dunkerton, 1995: Orthogonal rotation of spatial patterns derived from singular value decomposition analysis. *J. Climate*, **8**, 2631–2643.

Deser, C., 2000: On the teleconnectivity of the "Arctic oscillation". *Geophys. Res. Lett.*, **21**, 1141–1144.

Hartmann, D.L., 1995: A PV view of zonal flow vacillation. *J. Atmos. Sci.*, **52**, 2561–2576.

Hartmann, J.M., Wallace, V. Limpasuvan, D.W.J. Thompson and J.R. Holton, 2000: Can ozone depletion and global warming interact to produce rapid climate change? *Proc. National Acad. Sci.*, **97**, 1412–1417.

Hoskins, B. and P.J. Valdes, 1990: On the existence of storm-tracks, *J. Atmos. Sci.*, **47**, 1854–1864.

Itoh, H., 2002: True versus apparent Arctic oscillation. *Geophys. Res. Lett.*, **29**, 10.1029/2001GL013978.

Kimoto, M., F.-F. Jin, M. Watanabe and N. Yasutomi, 2001: Zonal-eddy coupling and a neutral mode theory for the Arctic oscillation. *Geophys. Res. Lett.*, **28**, 737–740.

Limpasuvan, V. and D.L. Hartmann, 2000: Wave-maintained annular modes of climate variability. *J. Climate*, **13**, 4414–4429.

SGKS Group, 1999: DCL-5.1 (in Japanese). GFD-DENNOU Club. [Available online at http://www.gfd-dennou.org/library/dcl/.]

Swamp Project, 1998: AGCM5 (in Japanese). GFD-DENNOU Club. [Available online at http://www.gfd-dennou.org/arch/agcm5/.]

Taguchi, M., T. Yamaga and S. Yoden, 2001: Internal variability of the troposphere-stratosphere coupled system in a simple global circulation model. *J. Atmos. Sci.*, **58**, 3184–3203.

——— and S. Yoden, 2002: A parameter-sweep experiment on the annular variability with a simple global circulation model. *J. Meteor. Soc. Japan*, **80**, 1077–1088.

Thompson, D.W.J. and J.M. Wallace, 1998: The Arctic oscillation signature in the wintertime geopotential height and temperature fields. *Geophys. Res. Lett.*, **25**, 1297–1300.

——— and J.M. Wallace, 2000: Annular modes in the extratropical circulation. Part I: Month-to-month variability. *J. Climate*, **13**, 1000–1016.

———, ——— and G.C. Hegerl, 2000: Annular modes in the extratropical circulation. Part II: Trends. *J. Climate*, **13**, 1018–1036.

Wallace, J.M., D.S. Gutzler, 1981: Teleconnections in the geopotential height field during the Northern Hemisphere winter. *Mon. Wea. Rev.*, **109**, 784–829.

Yamazaki, K. and Y. Shinya, 1999: Analysis of the Arctic oscillation simulated by AGCM. *J. Meteor. Soc. Japan*, **77**, 1287–1298.

Yoden, S., M. Shiotani and I. Hirota, 1987: Multiple planetary flow regimes in the Southern Hemisphere. *J. Meteor. Soc. Japan*, **65**, 571–586.